

**Anisotropic magnetic form factor in a detwinned single crystal of BaFe<sub>2</sub>As<sub>2</sub>**K. Kodama,<sup>1</sup> M. Ishikado,<sup>2</sup> S. Wakimoto,<sup>1</sup> K. Kihou,<sup>3</sup> C. H. Lee,<sup>3</sup> A. Iyo,<sup>3</sup> H. Eisaki,<sup>3</sup> and S. Shamoto<sup>1</sup><sup>1</sup>*Quantum Beam Science Center, Japan Atomic Energy Agency, Tokai, Ibaraki 319-1195, Japan*<sup>2</sup>*Comprehensive Research Organization for Science and Society (CROSS), Tokai, Ibaraki 319-1106, Japan*<sup>3</sup>*Nanoelectronics Research Institute, National Institute of Advanced Industrial Science and Technology, Tsukuba, Ibaraki 305-8562, Japan*

(Received 16 June 2014; revised manuscript received 26 September 2014; published 16 October 2014)

We have performed neutron diffraction measurements at 12 K on a single crystal of BaFe<sub>2</sub>As<sub>2</sub>, which serves as the parent compound of iron-based superconductors. To investigate the in-plane anisotropy of the magnetic form factor in the antiferromagnetic phase, the single crystal was detwinned. The magnetic structure factor and magnetic form factor are well explained by the spin densities comprising  $3d_{yz}$  electrons with a fraction of approximately 40% and electrons in the other four  $3d$  orbitals each with a fraction of approximately 15%. It is a direct observation of the largely anisotropic spin density relative to the small orthorhombic lattice distortion,  $(a - b)/(a + b) \sim 0.3\%$ .

DOI: [10.1103/PhysRevB.90.144510](https://doi.org/10.1103/PhysRevB.90.144510)

PACS number(s): 74.70.Xa, 75.25.-j, 75.30.Gw, 75.50.Ee

**I. INTRODUCTION**

In-plane anisotropy observed in the electronic properties of iron-based superconductors is one of the important issues in relation to the mechanism of superconductivity. The parent compound of iron-based superconductors exhibits a structural phase transition from tetragonal to orthorhombic structures with decreasing temperature, whereas the superconducting phase achieved by partial atomic substitution retains a tetragonal structure down to the lowest temperature. In the superconducting phase and the tetragonal phase of the parent compound, the electronic properties exhibit twofold symmetry in the FeAs layer although the crystal structure is tetragonal with fourfold symmetry [1]. Such in-plane anisotropy, which is the so-called nematic state, probably originates from the degrees of freedom of the electrons. The so-called spin nematic state and the orbital ordering are suggested as the origin of the strong breaking of fourfold symmetry [2–6].

In the orthorhombic phases of the parent compound and nonsuperconducting underdoped compounds, apparent in-plane anisotropy has been observed in both the electronic and magnetic properties. Electrical resistivity along the  $b$  direction is approximately twice the resistivity along the  $a$  direction in the orthorhombic phase of underdoped Ba(Fe<sub>1-x</sub>Co<sub>x</sub>)<sub>2</sub>As<sub>2</sub> [7,8]. Optical conductivity below about 0.2 cm<sup>-1</sup> along the  $a$  direction is also approximately twice the conductivity along the  $b$  direction in BaFe<sub>2</sub>As<sub>2</sub> [9,10]. A drastic change in Fermi surfaces with fourfold symmetry to that with twofold symmetry is observed below the antiferromagnetic transition temperature due to resolving a degeneracy between  $3d_{yz}$  and  $3d_{zx}$  orbitals [11,12]. The energy dispersion of the spin wave in the antiferromagnetic phase observed by inelastic neutron scattering exhibits large anisotropy, which is explained by considering the nearest neighboring magnetic interactions along the  $a$  and  $b$  directions with opposite sign [13–15]. These anisotropic behaviors observed in the orthorhombic phase are more pronounced than that simply expected from the small difference between the  $a$  and  $b$  lattice constants (less than 1%). These results suggest that the electronic state, for example, the spatial distribution of the  $3d$  electrons that contribute to the electronic and magnetic properties, is largely anisotropic. However, based on early neutron diffraction

measurements on a single crystal sample of the parent compound including twinned domains, it was reported that the magnetic form factor estimated from the magnetic Bragg intensities of  $h0l$  reflections is nearly isotropic [16], which is inconsistent with the above discussed anisotropic magnetic behaviors. In this paper, the results of neutron diffraction measurements on a detwinned single crystal of BaFe<sub>2</sub>As<sub>2</sub> in the antiferromagnetic phase are reported. The magnetic form factor determined from the magnetic Bragg intensities of both  $hkh$  and  $h0l$  reflections is anisotropic in the  $a$ - $b$  plane; this is qualitatively consistent with the anisotropic magnetic behaviors.

**II. EXPERIMENTS**

A single crystal of BaFe<sub>2</sub>As<sub>2</sub> was grown by the self-flux method. The details are reported in Ref. [16]. A crystal with dimensions 4 mm × 4 mm × 0.5 mm was used in the neutron diffraction measurements. The neutron diffraction measurements were performed using the triple-axis spectrometer TAS-1 installed at the research reactor JRR-3 of Japan Atomic Energy Agency. The single crystal was detwinned in a sample holder made of Al by uniaxial pressure along the  $b$  axis in the orthorhombic phase. For estimating the nuclear and magnetic Bragg intensities, the neutron absorption of the sample holder was corrected by considering the neutron flight paths in the sample holder for each Bragg reflection. The sample was sealed in an aluminum can, and then mounted in a closed-cycle He gas refrigerator. A collimation sequence of open-open-S-80'-open (where S denotes the sample) was employed. Pyrolytic graphites (PGs) were used for the monochromator and an analyzer. Another PG was placed downstream of the sample to eliminate higher order neutrons. The detwinning was confirmed at 12 K by a  $\theta$ - $2\theta$  scan with a neutron wavelength of 2.3532 Å, as shown in Fig. 1. The nuclear and magnetic Bragg reflections were collected by a  $\theta$ - $2\theta$  scan with a neutron wavelength of 1.6377 Å. The crystal was oriented in accordance with two types of configurations including the  $hkh$  and  $h0l$  reciprocal lattice points in the horizontal scattering planes.

**III. RESULTS AND DISCUSSION**

Figures 1(a) and 1(b) show the profiles of the 040 and 400 nuclear Bragg reflections obtained under the configurations

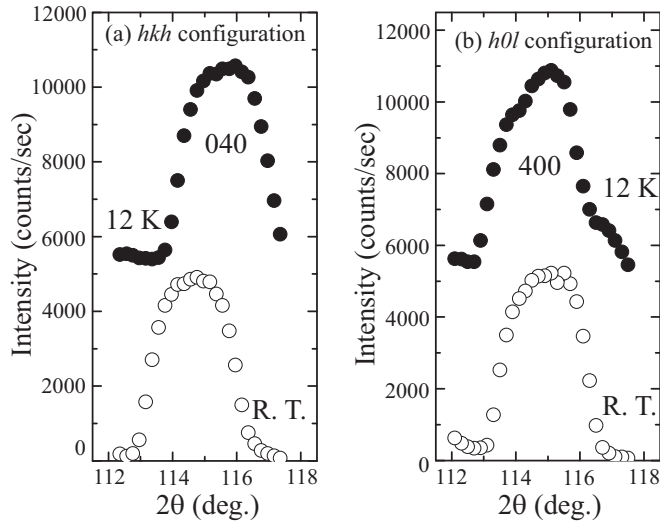


FIG. 1. Peak profiles of the (a) 040 and (b) 400 nuclear Bragg reflections obtained under the scattering configurations employed to collect the intensity of the  $hkh$  and  $h0l$  reflections, respectively. The data were collected at 12 K (solid circles) and room temperature (open circles).

employed to collect the intensity of the  $hkh$  and  $h0l$  reflections, respectively. The data were collected at room temperature and 12 K, where the crystal structures are tetragonal and orthorhombic, respectively. Here, because we use the notation of the orthorhombic structure, the reflections at room temperature correspond with 220 reflection in the tetragonal structure. The peak width at room temperature nearly corresponds with the instrumental resolution (momentum transfer of approximately  $0.1 \text{ \AA}^{-1}$  under the condition with a neutron wavelength of  $2.3532 \text{ \AA}$ ). The 040 and 400 reflections of the orthorhombic phase at 12 K are observed at different positions and their peak widths almost correspond with the width at room temperature, indicating that the detwinned single crystal is obtained at 12 K. The lattice constants at 12 K estimated

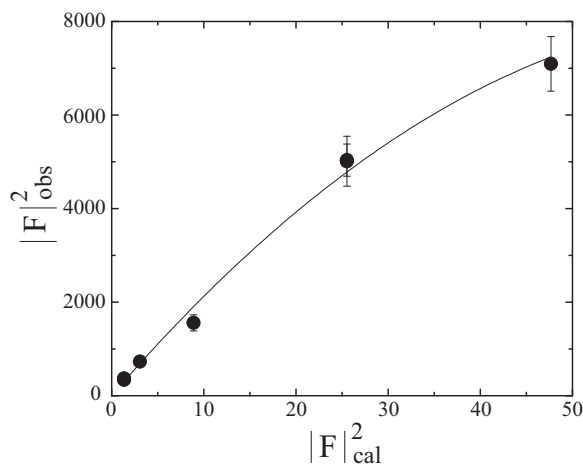


FIG. 2. Observed squared nuclear structure factor  $|F_N|_{\text{obs}}^2$  is plotted against squared nuclear structure factor  $|F_N|_{\text{cal}}^2$  calculated using the atomic positions reported in Ref. [18]. The solid line is the fitting result using the formula  $|F_N|_{\text{obs}}^2 = A|F_N|_{\text{cal}}^2(1 - B|F_N|_{\text{cal}}^2)$ .

from the positions of the peak centers of the 400, 040, and 002 reflections are  $a = 5.601 \text{ \AA}$ ,  $b = 5.568 \text{ \AA}$ , and  $c = 12.95 \text{ \AA}$ , respectively. In Fig. 2, the observed squared nuclear structure factor  $|F_N|_{\text{obs}}^2$  is plotted against the calculated squared structure factor  $|F_N|_{\text{cal}}^2$ . The observed data were corrected by the Lorentz factor  $L(\theta)$ . Here, we use the atomic positions reported for the orthorhombic phase in the calculation of  $|F_N|_{\text{cal}}^2$  [18]. The solid line is the fitting result using the formula  $|F_N|_{\text{obs}}^2 = A|F_N|_{\text{cal}}^2(1 - B|F_N|_{\text{cal}}^2)$ , where  $A$  is a scale factor and  $B$  accounts for extinction [19].

Using the scale factor  $A$  determined from the analysis of the nuclear Bragg intensities, the intensities of the magnetic Bragg reflections are described using the following equations:

$$I_{\text{obs}}(\mathbf{Q}) = A \times L(\theta) |F|_{\text{obs}}^2, \quad (1)$$

$$|F|_{\text{obs}}^2 = \gamma_0^2 \mu^2 f_{\text{obs}}(\mathbf{Q})^2 \times \left| \sum_n \sin \alpha_n \exp[2\pi i(hx_n + ky_n + lz_n)] \right|^2, \quad (2)$$

$$L(\theta) = 1/\sin 2\theta, \quad (3)$$

where the summation is taken over all magnetic moments in the magnetic unit cell and  $\gamma_0 = 0.269 \times 10^{-12} \text{ cm}$ ,  $\mu$  is the amplitude of the ordered magnetic moment in the unit of Bohr magneton, and  $\alpha$  is the angle between the direction of the  $n$ th magnetic moment and the scattering vector  $\mathbf{Q}$ . The magnetic structure in the antiferromagnetic phase has already been reported, as schematically shown in Fig. 3(a) [20–22]. The magnetic moments have antiferromagnetic and ferromagnetic arrangements along the  $a$  and  $b$  directions, respectively, and are nearly parallel to the  $a$  direction, which is the so-called stripe type magnetic structure. For this magnetic structure, the magnetic reflection is observed at  $hkl$  with  $h = 2n + 1$ ,  $k = 2n$ , and  $l = 2n + 1$ , where  $n$  is an integer. If we assume that the direction of the magnetic moment is slightly away from the  $a$  axis in the  $a$ - $b$  plane,  $\phi$ , as shown in Fig. 3(a), the magnetic structure factor depends on  $\phi$ , and Eq. (2) can be rewritten as follows:

$$|F|_{\text{obs}}^2 = 64\gamma_0^2 \mu^2 f_{\text{obs}}(\mathbf{Q})^2 \times \left| \sin \left\{ \cos^{-1} \left( \frac{ha^* \cos \phi + kb^* \sin \phi}{Q\mu} \right) \right\} \right|^2. \quad (4)$$

Although the observed squared magnetic structure factor  $|F|_{\text{obs}}^2$  and the observed magnetic form factor  $f_{\text{obs}}(\mathbf{Q})$  can be determined from the observed magnetic Bragg intensities and Eqs. (1), (3), and (4), the estimated value of the latter depends on  $\phi$ . Here we compare  $|F|_{\text{obs}}^2$  and  $f_{\text{obs}}(\mathbf{Q})$  with the calculated squared magnetic structure factor  $|F|_{\text{cal}}^2$  obtained by Eq. (4), whose subscript is replaced with “cal,” and the calculated magnetic form factor  $f_{\text{cal}}(\mathbf{Q})$  which is obtained by Eq. (5) as follows:

$$f_{\text{cal}}(\mathbf{Q}) = w_{yz} f_{yz}(\mathbf{Q}) + \frac{1 - w_{yz}}{4} \{f_{xy}(\mathbf{Q}) + f_{zx}(\mathbf{Q}) + f_{x^2-y^2}(\mathbf{Q}) + f_{3z^2-r^2}(\mathbf{Q})\}. \quad (5)$$

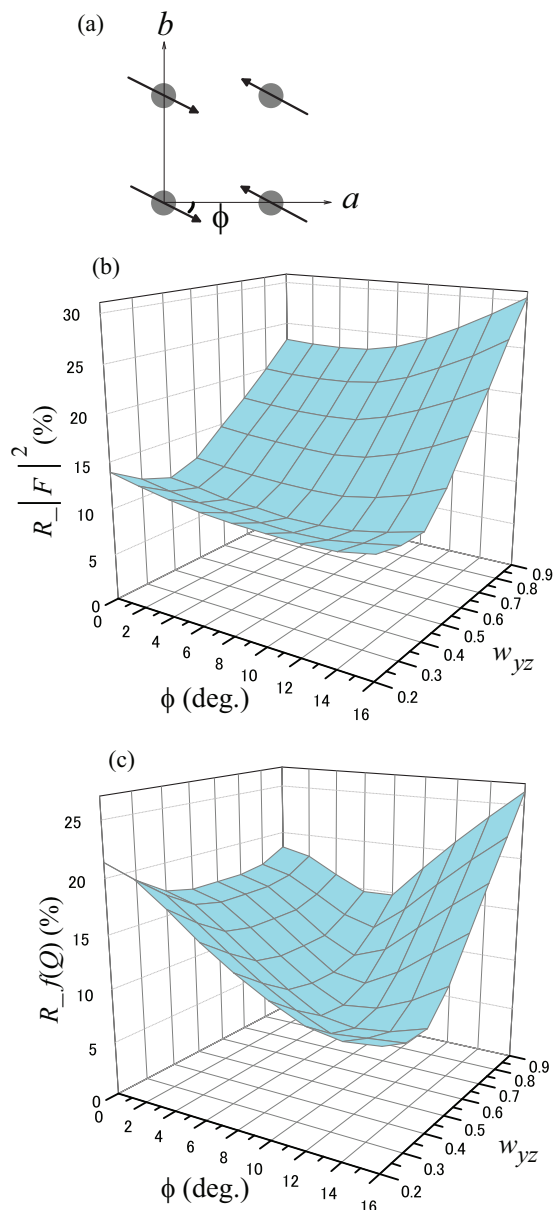


FIG. 3. (Color online) (a) Magnetic structure in the antiferromagnetic phase of BaFe<sub>2</sub>As<sub>2</sub>. (b)  $R$  factors estimated from  $|F|_{\text{obs}}^2$  and  $|F|_{\text{cal}}^2$ , and (c) those from  $f_{\text{obs}}(Q)$  and  $f_{\text{cal}}(Q)$  are plotted against  $\phi$  and  $w_{yz}$ .

Here the  $x$ ,  $y$ , and  $z$  directions correspond with the  $a$ ,  $b$ , and  $c$  directions of the orthorhombic lattice, respectively. Although the isotropic magnetic form factor has been reported [16], we consider the in-plane anisotropic form factor, which has a larger weight of the  $3d_{yz}$  orbital than the other orbitals because the decrease of  $f_{\text{obs}}(Q)$  with  $Q$  along the  $a^*$  direction is more gradual than the other directions, as shown later. In calculations using the above equations, the form factors and the wave functions of the  $3d$  orbitals reported for the Fe ion are used [23–25].

Figures 3(b) and 3(c) show the  $R$  factors estimated from  $|F|_{\text{obs}}^2$  and  $|F|_{\text{cal}}^2$ , and from  $f_{\text{obs}}(Q)$  and  $f_{\text{cal}}(Q)$ , for various  $\phi$  and  $w_{yz}$ , respectively. The  $R$  factors are estimated by the following equation,  $R = \sum_i |W_i^{\text{obs}} - W_i^{\text{cal}}| / \sum_i W_i^{\text{obs}}$ , where

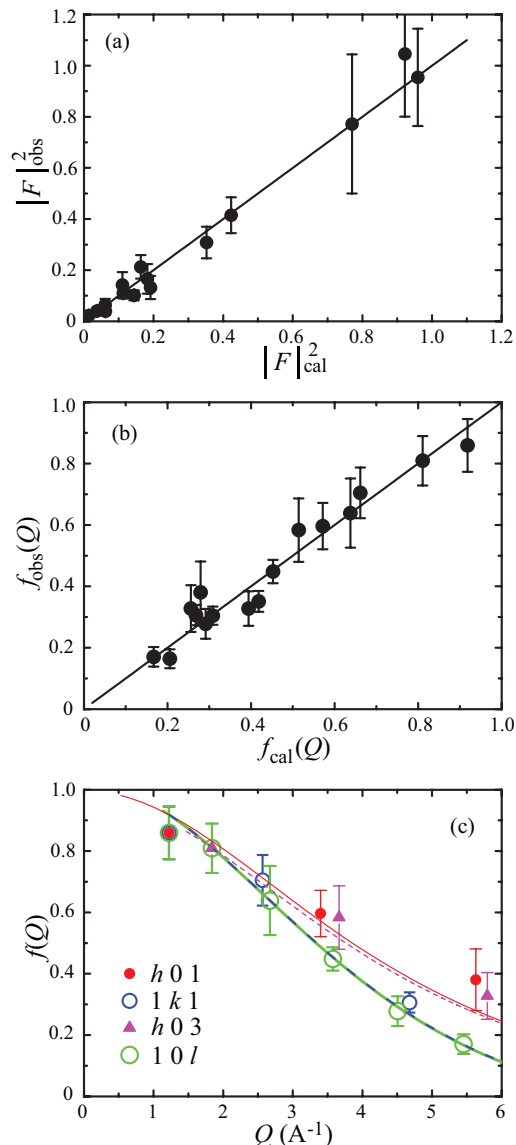


FIG. 4. (Color online) (a)  $|F|_{\text{obs}}^2$  and (b)  $f_{\text{obs}}(Q)$  are plotted against  $|F|_{\text{cal}}^2$  and  $f_{\text{cal}}(Q)$ , respectively. Straight lines indicate that  $|F|_{\text{obs}}^2 = |F|_{\text{cal}}^2$  and  $f_{\text{obs}}(Q) = f_{\text{cal}}(Q)$ . (c) The  $f_{\text{obs}}(Q)$  obtained at  $h01$  (solid circles),  $1k1$  (small open circles),  $h03$  (solid triangles), and  $10l$  (large open circles) reflections are plotted against  $Q$ . Thin solid and dashed lines represent the magnetic forms factors calculated at  $h01$  and  $h03$ , and bold dashed and solid lines are the magnetic form factors calculated at  $1k1$  and  $10l$ , respectively. The bold dashed line corresponds with the bold solid line. (d) A schematic representation of the spin density of Fe ions in the orthorhombic unit cell in the  $a$ - $b$  plane.

$W_i^{\text{obs}}$  and  $W_i^{\text{cal}}$  are the observed and calculated values of the squared magnetic structure factors and magnetic form factors, respectively.  $\sum_i$  indicates a summation taken over all observed magnetic Bragg reflections. The  $R$  factor for the squared magnetic structure factor has a minimum value of 9.4% at  $\phi = 10^\circ$  and  $w_{yz} = 0.4$ , and that for the magnetic form factor has a minimum value of 8.0% at  $\phi = 12^\circ$  and  $w_{yz} = 0.4$ . The values of  $\phi$  and  $w_{yz}$ , where the  $R$  factor obtained from  $|F|_{\text{obs}}^2$  and  $|F|_{\text{cal}}^2$  is minimum, are consistent with those where the  $R$  factor obtained from  $f_{\text{obs}}(\mathbf{Q})$  and  $f_{\text{cal}}(\mathbf{Q})$  is minimum. The weight of the  $3d_{yz}$  orbital is larger than those of any other  $3d$  orbitals ( $w_{yz}$  is approximately 0.4 and the other weights are approximately 0.15). This indicates that such an anisotropic magnetic form factor must be considered to reproduce the observed magnetic structure factor and magnetic form factor. In Figs. 4(a) and 4(b),  $|F|_{\text{obs}}^2$  and  $f_{\text{obs}}(\mathbf{Q})$  are plotted against  $|F|_{\text{cal}}^2$  and  $f_{\text{cal}}(\mathbf{Q})$ , respectively. The plotted values are obtained for  $\phi = 10^\circ$  and  $w_{yz} = 0.4$ . Here we adopt the amplitude of the magnetic moment,  $\mu = 0.70\mu_B$ , optimized in the above analysis. The observed values are closely reproduced by the calculated values, and the  $R$  factors are 9.4% and 8.4% for the squared magnetic structure factor and the magnetic form factor, respectively. In Fig. 4(c), the  $Q$  dependences of the observed magnetic form factors at the  $h01$ ,  $1k1$ ,  $h03$ , and  $10l$  reflections estimated using the above  $\phi$ ,  $w_{yz}$ , and  $\mu$  values are shown by solid circles, small open circles, solid triangles, and large open circles, respectively. The  $Q$  dependence of  $f_{\text{obs}}(\mathbf{Q})$  at  $1k1$  nearly corresponds with that of the  $10l$  reflections. The decreases in  $Q$  of  $f_{\text{obs}}(\mathbf{Q})$  at the  $h01$  and  $h03$  reflections are more gradual than those at the  $1k1$  and  $10l$  reflections. The lines that show the magnetic form factors calculated for the above reciprocal lattice points nearly reproduce  $f_{\text{obs}}(\mathbf{Q})$ . From these analyses, we conclude that the magnetic form factor exhibits in-plane anisotropy. A schematic of the spin density expected from the obtained magnetic form factor is shown in Fig. 4(d).

The earlier neutron diffraction study on  $\text{SrFe}_2\text{As}_2$  has claimed that the magnetic form factor is approximately isotropic [16], which is inconsistent with our results. In their data, the magnetic form factor at the 501 reflection is zero. We speculate that the obvious magnetic Bragg peak of the 501 reflection could not be detected in their experimental accuracy, because the structure factor of the 501 reflection is considerably smaller than the intensities at the reciprocal lattice points with larger  $l$  values. If the 501 reflection had been detected, their magnetic form factor would have exhibited in-plane anisotropy similar to our result, because the decrease with  $Q$  of the magnetic form factor at  $h01$  with  $h = 1$  and 3 is also slower than those at the other reciprocal lattice points, for example,  $10l$  in their data.

The present study directly shows the anisotropic spin density in the  $a$ - $b$  plane. The magnetic contribution from

the  $3d_{yz}$  electron is more than twice that from the  $3d_{zx}$  electron. The difference in the magnetic contribution between the  $3d_{yz}$  and  $3d_{zx}$  orbitals that provide the in-plane anisotropy is pronounced relative to the small orthorhombic lattice distortion,  $(a - b)/(a + b) \sim 0.3\%$ . The anisotropic electronic structure has been observed by photon polarization of the angle-resolved photoemission spectroscopy (ARPES) measurements [11,12]. The splitting between the  $3d_{yz}$  and  $3d_{zx}$  orbitals reaches approximately 60 meV, leading to a possible occupational difference of 18% between these orbitals but without any spin polarization information [12]. On the other hand, our result directly shows the spin density in which the magnetic moment of the  $3d_{yz}$  electrons is more than twice that of the  $3d_{zx}$  electrons. The present result provides us with a further understanding of the anisotropic electronic state.

An orbital ordering model based on a first-principles Wannier function analysis is proposed [5], where the magnetic moment originates mainly from the  $3d_{yz}$  orbital and partially from the  $3d_{zx}$  orbital. In such an orbital ordering state, the nearest neighbor antiferromagnetic interaction along the  $b$  direction is negligibly small relative to the interactions along the  $a$  and  $[111]$  directions, reproducing the stripe type magnetic structure and the large anisotropy of the spin wave dispersion. In the quantitative calculation on the spin polarization, the ratio of the magnetic moment of the  $3d_{zx}$  electrons to that of the  $3d_{yz}$  electrons is 0.40, in good agreement with that of the spin density obtained by our present study (0.38). On the other hand, the spin nematic model in which the magnetic fluctuation plays a major role of the strong breaking fourfold symmetry is also suggested [2,6]. In such a model, the different occupancies between the  $3d_{yz}$  and  $3d_{zx}$  orbitals leading to the different magnetic moments are also driven, which is qualitatively consistent with our anisotropic spin density.

#### IV. SUMMARY

The magnetic structure factor and the magnetic form factor that have been determined in the present study by neutron diffraction measurements on a detwinned single crystal of  $\text{BaFe}_2\text{As}_2$  can be explained by considering that approximately half of the magnetic moment is contributed from the electrons in the  $3d_{yz}$  orbital. In the antiferromagnetic phase, the spin density has a large anisotropy in the  $a$ - $b$  plane whereas the orthorhombic lattice distortion is very small.

#### ACKNOWLEDGMENTS

This work was supported by JST, TRIP. Furthermore, this work was supported by the JSPS KAKENHI Grants No. 25287094 and No. 24340090.

[1] S. Kasahara, H. J. Shi, K. Hashimoto, S. Tonegawa, Y. Mizukami, T. Shibauchi, K. Sugimoto, T. Fukuda, T.

Terashima, A. H. Nevidomskyy, and Y. Matsuda, *Nature (London)* **486**, 382 (2012).

- [2] R. M. Fernandes, A. V. Chubukov, J. Knolle, I. Eremin, and J. Schmalian, *Phys. Rev. B* **85**, 024534 (2012).
- [3] F. Krüger, S. Kumar, J. Zaanen, and J. van den Brink, *Phys. Rev. B* **79**, 054504 (2009).
- [4] W. Lv, J. Wu, and P. Phillips, *Phys. Rev. B* **80**, 224506 (2009).
- [5] C. C. Lee, W.-G. Yin, and W. Ku, *Phys. Rev. Lett.* **103**, 267001 (2009).
- [6] R. M. Fernandes, A. V. Chubukov, and J. Schmalian, *Nat. Phys.* **10**, 97 (2014).
- [7] J.-H. Chu, J. G. Analytis, K. D. Greve, P. L. McMahon, Z. Islam, Y. Yamamoto, and I. R. Fisher, *Science* **329**, 824 (2010).
- [8] S. Ishida, M. Nakajima, T. Liang, K. Kihou, C. H. Lee, A. Iyo, H. Eisaki, T. Kakeshita, Y. Tomioka, T. Ito, and S. Uchida, *Phys. Rev. Lett.* **110**, 207001 (2013).
- [9] M. Nakajima, T. Liang, S. Ishida, Y. Tomioka, K. Kihou, C. H. Lee, A. Iyo, H. Eisaki, T. Kakeshita, T. Ito, and S. Uchida, *Proc. Natl. Acad. Sci. USA* **108**, 12238 (2011).
- [10] M. Nakajima, S. Ishida, Y. Tomioka, K. Kihou, C. H. Lee, A. Iyo, T. Ito, T. Kakeshita, H. Eisaki, and S. Uchida, *Phys. Rev. Lett.* **109**, 217003 (2012).
- [11] T. Shimojima, K. Ishizaka, Y. Ishida, N. Katayama, K. Ohgushi, T. Kiss, M. Okawa, T. Togashi, X.-Y. Wang, C.-T. Chen, S. Watanabe, R. Kadota, T. Oguchi, A. Chainani, and S. Shin, *Phys. Rev. Lett.* **104**, 057002 (2010).
- [12] M. Yi, D. Lu, J.-H. Chu, J. G. Analytis, A. P. Sorini, A. F. Kemper, B. Moritz, S.-K. Mo, R. G. Moore, M. Hashimoto, W.-S. Lee, Z. Hussain, T. P. Devereaux, I. R. Fisher, and Z.-X. Shen, *Proc. Natl. Acad. Sci. USA* **108**, 6878 (2011).
- [13] J. Zhao, D. T. Adroja, D.-X. Yao, R. Bewley, S. Li, X. F. Wang, G. Wu, X.-H. Chen, J. Hu, and P. Dai, *Nat. Phys.* **5**, 555 (2009).
- [14] R. A. Ewings, T. G. Perring, J. Gillett, S. D. Das, S. E. Sebastian, A. E. Taylor, T. Guidi, and A. T. Boothroyd, *Phys. Rev. B* **83**, 214519 (2011).
- [15] L. W. Harriger, H. Q. Luo, M. S. Liu, C. Frost, J. P. Hu, M. R. Norman, and P. Dai, *Phys. Rev. B* **84**, 054544 (2011).
- [16] W. Ratcliff, P. A. Kienzle, J. W. Lynn, S. Li, P. Dai, G. F. Chen, and N. L. Wang, *Phys. Rev. B* **81**, 140502 (2010).
- [17] M. Nakajima, S. Ishida, K. Kihou, Y. Tomioka, T. Ito, Y. Yoshida, C. H. Lee, H. Kito, A. Iyo, H. Eisaki, K. M. Kojima, and S. Uchida, *Phys. Rev. B* **81**, 104528 (2010).
- [18] M. Rotter, M. Tegel, D. Johrendt, I. Schellenberg, W. Hermes, and R. Pöttgen, *Phys. Rev. B* **78**, 020503 (2008).
- [19] S. Shamoto, M. Sato, J. M. Tranquada, B. J. Sternlieb, and G. Shirane, *Phys. Rev. B* **48**, 13817 (1993).
- [20] J. Zhao, W. Ratcliff, J. W. Lynn, G. F. Chen, J. L. Luo, N. L. Wang, J. Hu, and P. Dai, *Phys. Rev. B* **78**, 140504 (2008).
- [21] Q. Huang, Y. Qiu, W. Bao, M. A. Green, J. W. Lynn, Y. C. Gasparovic, T. Wu, G. Wu, and X. H. Chen, *Phys. Rev. Lett.* **101**, 257003 (2008).
- [22] A. I. Goldman, D. N. Argyriou, B. Ouladdiaf, T. Chatterji, A. Kreyssig, S. Nandi, N. Ni, S. L. Bud'ko, P. C. Canfield, and R. J. McQueeney, *Phys. Rev. B* **78**, 100506 (2008).
- [23] A. J. Freeman, *Acta Crystallogr.* **12**, 261 (1959).
- [24] A. J. Freeman, *Phys. Rev.* **113**, 169 (1959).
- [25] R. E. Watson and A. J. Freeman, *Acta Crystallogr.* **14**, 27 (1961).